Frequent loss-of-heterozygosity in CRISPR-Cas9-edited early human embryos

Gregorio Alanis-Lobato[a], Jasmin Zohren[b], Afshan McCarthy[a], Norah M.E. Fogarty[a,c], Nada Kubikova[d], Emily Hardman[a], Maria Greco[e], Dagan Wells[d,f], James M.A. Turner[b], Kathy K. Niakan[a,*]

[a]Human Embryo and Stem Cell Laboratory, The Francis Crick Institute, 1 Midland Road, London NW1 1AT, UK

[b]Sex Chromosome Biology Laboratory, The Francis Crick Institute, 1 Midland Road, London NW1 1AT, UK

[c]Centre for Stem Cells and Regenerative Medicine, King's College London, Guy's Campus, Great Maze Pond, London SE1 9RT, UK

[d]University of Oxford, Winchester House, Heatley Road, Oxford Science Park, Oxford OX4 4GE, UK

[e]Ancient Genomics Laboratory, The Francis Crick Institute, 1 Midland Road, London NW1 1AT, UK

[f]Juno Genetics, Winchester House, Heatley Road, Oxford Science Park, Oxford OX4 4GE, UK

To whom correspondence should be addressed:

Kathy K. Niakan

Human Embryo and Stem Cell Laboratory

The Francis Crick Institute

1 Midland Road

London NW1 1AT

UK

kathy.niakan@crick.ac.uk

Keywords: genome editing, CRISPR-Cas9, human embryo, segmental aneuploidy, loss-of-heterozygosity

Abstract

CRISPR-Cas9 genome editing is a promising technique for clinical applications, such as the correction of disease-associated alleles in somatic cells. The use of this approach has also been discussed in the context of heritable editing of the human germline. However, studies assessing gene correction in early human embryos report low efficiency of mutation repair, high rates of mosaicism and the possibility of unintended editing outcomes that may have pathologic consequences. We developed computational pipelines to assess single-cell genomics and transcriptomics datasets from OCT4 (*POU5F1*) CRISPR-Cas9-targeted and Cas9-only control human preimplantation embryos. This allowed us to evaluate on-target mutations that would be missed by more conventional genotyping techniques. We observed loss-of-heterozygosity in edited cells that spanned regions beyond the *POU5F1* on-target locus, as well as segmental loss and gain of chromosome 6, on which the *POU5F1* gene is located. Unintended genome editing outcomes were present in approximately 22% of the human embryo cells analysed and spanned 4 to 20kb. Our observations are consistent with recent findings indicating complexity at on-target sites following CRISPR-Cas9 genome editing. Our work underscores the importance of further basic research to assess the safety of genome editing techniques in human embryos, which will inform debates about the potential clinical use of this technology.

Introduction

Clustered regularly interspaced short palindromic repeat (CRISPR)-CRISPR associated 9 (Cas9) genome editing is not only an indispensable molecular biology technique (1) but also has enormous therapeutic potential as a tool to correct disease-causing mutations (2). Genome editing of human embryos or germ cells to produce heritable changes has the potential to reduce the burden of genetic disease and its use in this context is currently a topic of international debate centred around ethics, safety and efficiency (3, 4).

Several groups have conducted studies to assess the feasibility of gene correction in early human embryos (5–7) and they all encountered low efficiency of gene repair and high levels of mosaicism (i.e. embryos with corrected as well as mutant blastomeres), both unacceptable outcomes for clinical applications. In 2017, Ma *et al.* set out to correct a 4bp pathogenic heterozygous deletion in the *MYBPC3* gene using the CRISPR-Cas9 system (8). After fertilising healthy wild-type (WT) oocytes with presumed equal numbers of WT and mutant (Mut) spermatozoa, they microinjected 54 S-phase zygotes with a mixture of Cas9 protein, a single guide RNA (sgRNA) that specifically targeted the mutant sequence and a repair template with two synonymous single nucleotide variants that would allow them to confirm the gene correction (8). Rather than the expected 50/50 percent ratio of healthy (WT/WT) and heterozygous (WT/Mut) embryos, results suggested that 66.7% of embryos were uniformly homozygous (WT/WT), while 24% were mosaic (different genotypes in individual cells) and 9.3% were uniformly WT/Mut embryos (i.e. presumed unedited). Moreover, co-injection of the editing components with sperm into 58 M-phase oocytes produced 72.4% uniformly homozygous embryos, with the rest exhibiting insertion-deletion (indel) mutations in the paternal allele caused by non-homologous end-joining (NHEJ). Intriguingly, the excess of uniformly homozygous embryos in both cases was not associated with use

of the provided repair template for gene correction. Instead, the authors suggest that in edited embryos the WT maternal allele served as template for the high-fidelity homology directed repair (HDR) mechanism to repair the double-strand lesion caused by the Cas9 protein in the paternal allele (8).

Ma and colleagues' interpretation of gene editing by inter-homologue homologous recombination (IH-HR) in the early human embryo has been met with scepticism because alternative phenomena can account for the observed results (9–11). One possible explanation is that the CRISPR-Cas9 system can induce large deletions and complex genomic rearrangements with pathogenic potential at the on-target site (9, 10, 12–14). These events can be overlooked because genotyping of the targeted genomic locus often involves the amplification of a small PCR fragment around the on-target cut-site. CRISPR-Cas9-induced deletions larger than these fragments in either direction would eliminate one or both PCR primer annealing sites. This in turn can lead to amplification of only one allele, giving the false impression that targeting was unsuccessful or that there is a single homozygous event at the on-target site (9, 10, 15). Loss-of-heterozygosity (LOH) can also be the result of more complex genomic rearrangements like inversions, large insertions, translocations, chromosome loss and even IH-HR with crossover, whereby a large piece of one parental allele is integrated by the other parental chromosome at the on-target cut-site (15).

The reported frequencies of unintended CRISPR-Cas9 on-target damage are not negligible. Adikusama *et al.* targeted six genes in a total of 127 early mouse embryos and detected large deletions (between 100bp and 2.3kb) in 45% of their samples using long-range PCR (10). Of note, large deletions were generally more prevalent when they targeted intronic regions (>70%) than when they targeted exons (20%). Consistent with this, Kosicki and colleagues observed large deletions (up to 6kb) and other complex genomic lesions at frequencies of 5-20% of their clones after targeting the *PigA* and *Cd9* loci in two mouse embryonic stem cell (mESC) lines and primary mouse cells from the bone marrow, as well as the *PIGA* gene in immortalised human female retinal pigment epithelial cells (12). Moreover, Owens *et al.* used CRISPR-Cas9 with two sgRNAs to delete 100-150bp in the *Runx1* locus of mESCs and found that 23% of their clones had large deletions (up to 2kb) that escaped genotyping by short-range PCR (giving the impression that they were homozygous WT clones), with these complex on-target events becoming evident using long-range PCR (14). Similar damage and frequencies were also observed with the $Cas9^{D10A}$ nickase (11). More dramatic events were identified by Cullot *et al.*, who CRISPR-targeted the *UROS* locus in HEK293T and K562 cells for HDR correction with a repair template (13). Their experiments suggest that CRISPR-Cas9 can induce mega-base scale chromosomal truncations (~10% increase compared to controls). However, these cells have abnormal karyotypes and are p53 deficient, which may impact on their DNA damage repair machinery. In fact, they did not see the same effect in human foreskin fibroblasts but knocking-out of *TP53* in these primary cells increased the large deletion events by 10-fold (13).

Our lab used CRISPR-Cas9 genome editing to investigate the function of the pluripotency factor OCT4 (encoded by the *POU5F1* gene on the p-arm of chromosome 6) during human preimplantation development (16). We generated a number of single-cell amplified genomic DNA (gDNA) samples for genotyping and confirmed on-target genome editing in all microinjected embryos and a stereotypic indel pattern with the

majority of samples exhibiting a 2bp or 3bp homozygous deletion (16). However, we noted that in 5 of the samples analysed, the genotype could not be determined because of failures to PCR amplify the on-target genomic fragment. This finding suggested complexity at the on-target region that may have abolished one or both PCR primer binding sites. Moreover, we identified that 57 of the 137 successfully genotyped samples (42%) exhibited a WT/WT genotype based on PCR amplification of a short genomic fragment (16). We originally interpreted these cases as unsuccessful targeting events, however, given the frequencies of the on-target complexities noted above, we speculated that our previous methods may have missed more complex on-target events.

Here, we have developed computational pipelines to analyse low-pass whole genome sequencing (WGS), transcriptome and deep-amplicon sequencing data to assess the prevalence of LOH events in the context of CRISPR-Cas9-edited early human embryos (Fig. 1). Our results indicate that LOH events on chromosome 6, including chromosomal and segmental copy number abnormalities, are more prevalent in OCT4-edited embryos compared to Cas9-injected controls, adding to the growing body of literature reporting that CRISPR-Cas9 genome editing can cause unintended on-target damage.

Results

Segmental losses and gains at a CRISPR-Cas9 on-target site identified by cytogenetics analysis

In our previous study (16), *in vitro* fertilised zygotes donated as surplus to infertility treatment were microinjected with either an sgRNA-Cas9 ribonucleoprotein complex to target *POU5F1* or Cas9 protein alone as a control and cultured for up to 6 days (targeted and control samples, respectively). We collected a single cell or a cluster of 2-5 cells from these embryos for cytogenetic, genotyping or transcriptomic analysis (Fig. 1).

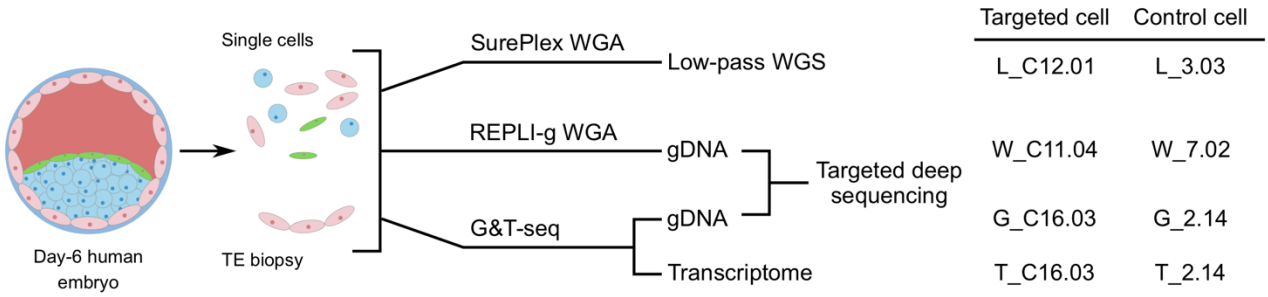

Fig. 1. Sample types and nomenclature used throughout the paper. We reanalysed low-pass whole genome sequencing (WGS) and transcriptome data from OCT4-targeted and Cas9 control single cells or trophectoderm (TE, precursor cells of the placenta) biopsies from human embryo samples. In addition, the genomic DNA (gDNA) isolated from single cells or TE biopsies subjected to the G&T-seq protocol or to whole genome amplification (WGA) was used for targeted deep sequencing across the *POU5F1* locus. Sample identifiers start with a prefix, followed by the embryo and cell number. The embryo number of CRISPR-edited samples is preceded by a letter C. Prefix L_ corresponds to the low-pass WGS data, prefix W_ to gDNA that was amplified with the REPLI-g kit, prefix G_ to gDNA extracted with the G&T-seq protocol and prefix T_ to scRNA-seq data produced with G&T-seq.

To determine whether CRISPR-Cas9 genome editing leads to complex on-target DNA damage that would have been missed by our previous targeted amplicon sequencing, we reanalysed low-pass WGS data following whole-genome amplification (WGA) from 23 OCT4-targeted and 8 Cas9 control samples (Table S1). Here and below, the prefix that distinguishes the processing steps is followed by an embryo number and a cell number. The samples used for low-pass WGS were identified with prefix L_ (Fig. 1). The letter C precedes the embryo number to distinguish CRISPR-Cas9 targeted from control samples (Fig. 1). Low-pass WGS data were used to generate copy number profiles for each sample to investigate the presence of abnormalities with a focus on chromosome 6 (Fig. 2A).

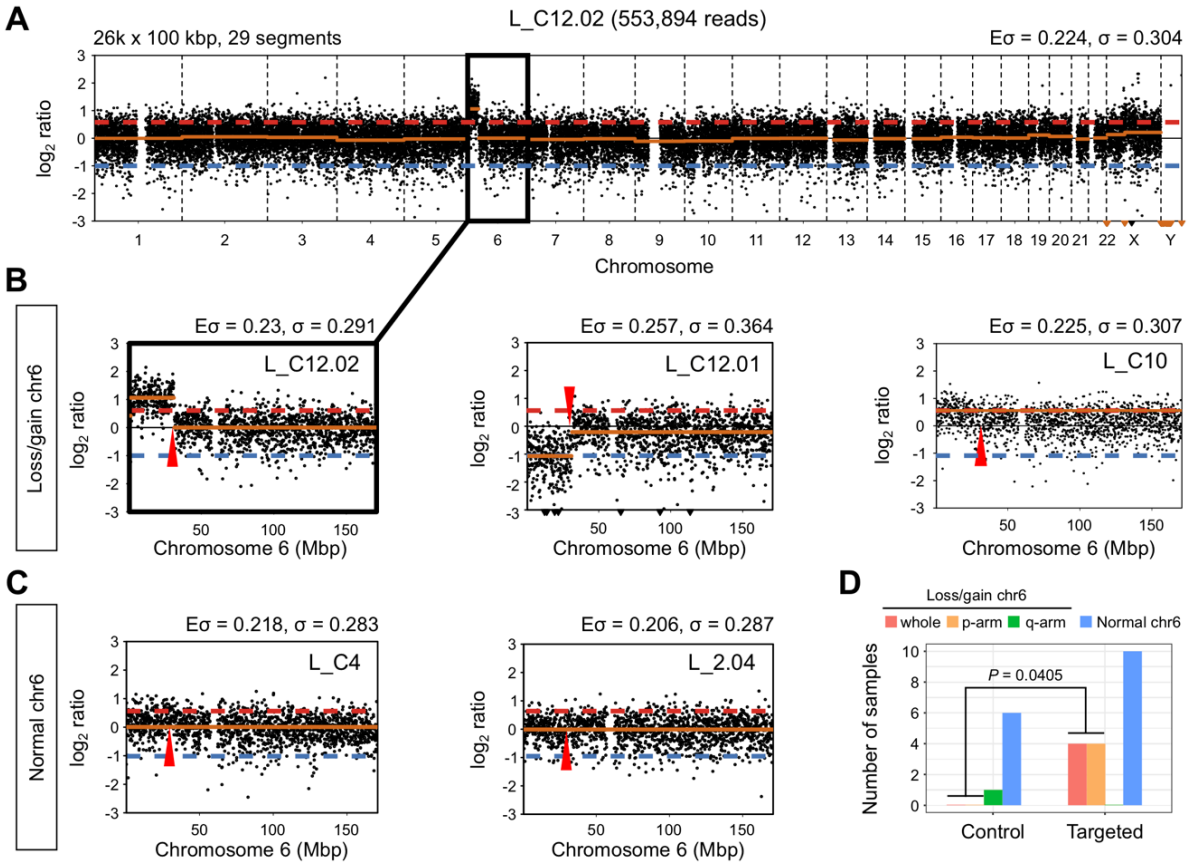

Fig. 2. Segmental losses/gains of chromosome 6 are prevalent in OCT4-targeted embryo samples. *(A)* Copy number profile of sample L_C12.02. The segmental gain of chromosome 6 is highlighted. The profile was constructed with 26,000 bins of size 100 kbp, which produced 29 segments. The expected (Eσ) and measured (σ) standard deviation of the profile are reported. *(B)* Zoomed-in view of the copy number profile for samples with segmental losses or gains of chromosome 6. *(C)* Zoomed-in view of the copy number profile for samples with normal chromosome 6. The Eσ and σ reported in B and C correspond to the chromosome only. The approximate position of the *POU5F1* gene is indicated by a red arrow. The red dashed line indicates a copy ratio of 3:2, while the blue dashed lines corresponds to a copy ratio of 1:2. *(D)* The number of control and targeted samples with whole or segmental losses/gains of chromosome 6 according to their copy number profiles. The reported p-value is the result of a one-tailed Fisher's test.

After pre-processing and quality control, we examined the profiles of 25 samples (18 CRISPR-Cas9 targeted and 7 Cas9 controls, Figs. S1A and S1B). 16 samples exhibited two copies of chromosome 6 with no obvious cytogenetic abnormalities (Figs. 2C, 2D and S2). 10 of the CRISPR-Cas9 target samples, or 55.6%, had no evidence of abnormalities on chromosome 6. By contrast, we observed that 8 out of the 18 targeted samples

had evidence of abnormalities on chromosome 6. 4 targeted samples presented a segmental loss or gain that was directly adjacent to or within the *POU5F1* locus on the p-arm of chromosome 6 (Figs. 2B, 2D and S2). Interestingly, this included two cells from the same embryo where one exhibited a gain and the other a reciprocal loss extending from 6p21.3 to the end of 6p (Fig. 2B). Altogether, segmental abnormalities were detected in 22.2% of the total number of CRISPR-Cas9 targeted samples that were evaluated. We also observed that 4 targeted samples had evidence of a whole gain of chromosome 6 (Figs. 2B, 2D and S2), which also represents 22.2% of the targeted samples examined. Conversely, a single Cas9 control sample had evidence of a segmental gain on the q-arm of chromosome 6, which was at a site distinct from the *POU5F1* locus (Fig. S2).

The number of segmental and whole-chromosome abnormalities observed in the CRISPR-Cas9 targeted human cells was significantly higher than in the control samples (Fig. 2D, $P = 0.0405$, one-tailed Fisher's test). Moreover, this significant difference can be attributed to the observed segmental abnormalities on 6p, because excluding them from the comparison results in a negligible difference in whole-chromosome abnormalities between targeted and control samples ($P = 0.2419$, one-tailed Fisher's test). This conclusion is further supported by the fact that none of the targeted samples show segmental losses or gains on the p-arm of chromosomes 5 and 7, the closest in size to chromosome 6, but the frequency of whole chromosome abnormalities is similar to that observed for chromosome 6, suggesting that genome editing does not exacerbate the rates of whole chromosome errors (Fig. S1C). Altogether, low-pass WGS analysis suggests that a significant proportion of unexpected on-target events leads to segmental abnormalities following CRISPR-Cas9 genome editing in human preimplantation embryos.

Loss-of-heterozygosity identified by targeted deep sequencing

The copy-number profiles described above with low-pass WGS data can only provide a coarse-grained karyotype analysis. To independently investigate the prevalence of LOH events at finer resolution and increased sequencing depth, we designed PCR primer pairs to amplify 15 fragments spanning a ~20kb region containing the *POU5F1* locus. We also included a control PCR amplification in the *ARGFX* locus located on chromosome 3 (Table S4). The PCR amplicons were used to perform deep sequencing by Illumina MiSeq using the gDNA isolated and amplified from 137 single cells or a cluster of 2-5 microdissected cells (111 CRISPR-Cas9 targeted and 26 Cas9 controls) (Fig. 1 and Table S2). The prefix W_ distinguished samples whose gDNA was isolated solely for WGA and the prefix G_ was used to demarcate samples that underwent WGA via the G&T-seq protocol (17). All of these samples were different from the samples used for the cytogenetic analyses above.

We then took advantage of the high coverage obtained at each of the sequenced fragments to call single nucleotide polymorphisms (SNPs), which allowed us to identify samples with putative LOH events: cases in which heterozygous variants, indicative of contribution from both parental alleles, cannot be confidently called in the amplicons flanking the CRISPR-Cas9 on-target site directly. Since we do not have the parental genotype from any of the samples that we analysed, we cannot exclude the possibility that they inherited a homozygous

genotype. Therefore, we required the presence of heterozygous SNPs in at least one additional cell from the same embryo to call putative LOH events.

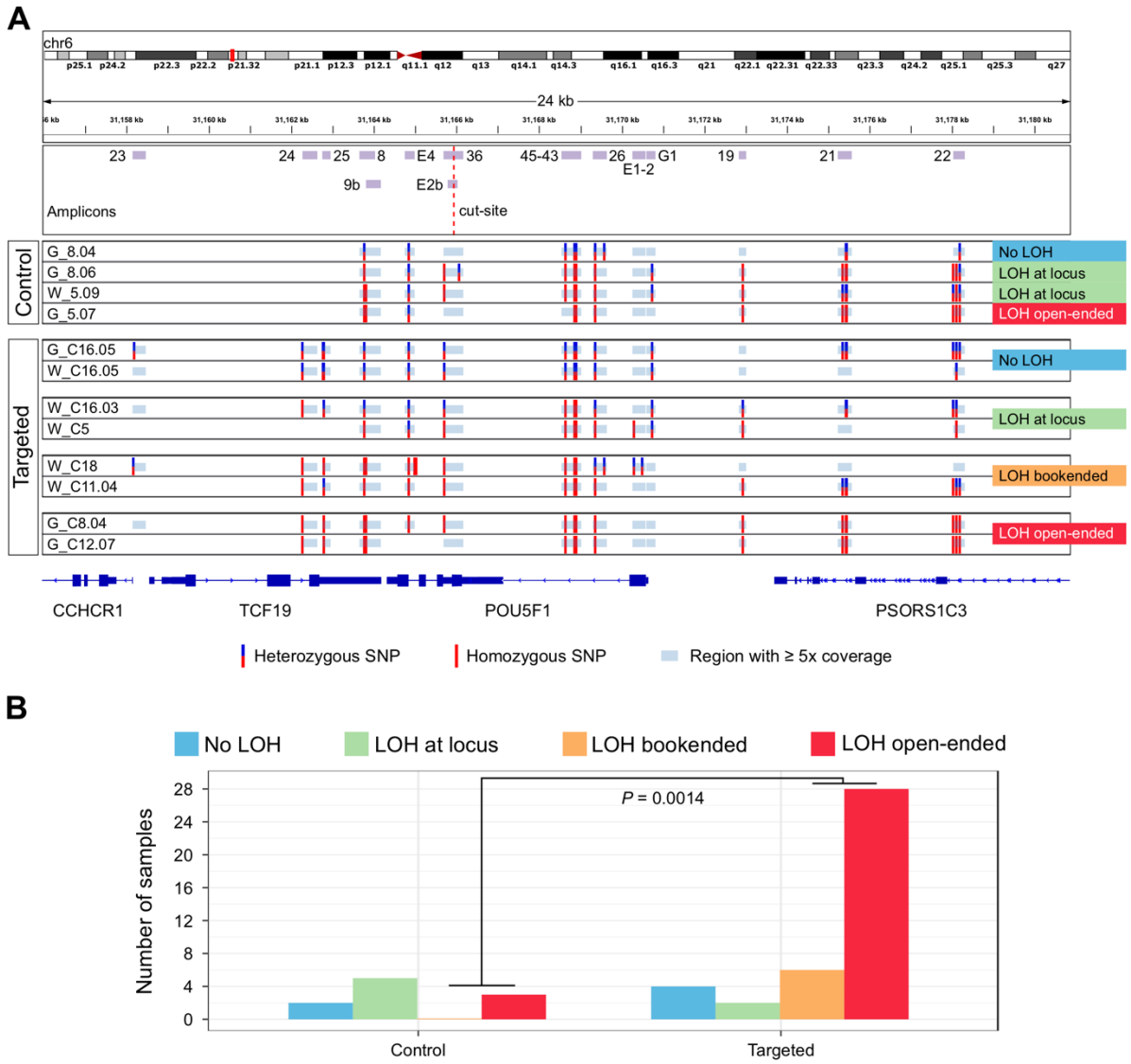

Fig. 3. LOH in the *POU5F1* locus is prevalent among OCT4-targeted embryo samples. *(A)* Single nucleotide polymorphism (SNP) profiles constructed from deep sequencing of the depicted amplicons. The four types of loss-of-heterozygosity (LOH) events observed are exemplified. Note that there are amplicons with ≥5x coverage in which SNPs were not called because all reads agree with the reference genome. *(B)* The frequency of each type of LOH event in control and targeted samples. The reported p-value is the result of a one-tailed Fisher's test.

The variant-calling pipeline that we implemented was specifically adjusted for MiSeq data from single cell amplified DNA and includes stringent pre-processing and filtering of the MiSeq reads (Methods). In addition, we only considered samples with ≥ 5x coverage in at least two thirds of the amplicons (Fig. S3). This threshold allowed us to retain as many samples as possible and still be confident in the SNP calling step (18). Thus, we proceeded with 40 CRISPR-Cas9 targeted and 10 Cas9 control samples with reliable SNP profiles for subsequent analysis. These data led to the identification of four different patterns: samples without clear evidence of LOH, samples with LOH at the on-target site, bookended and open-ended LOH events (Fig. 3A and Figs. S4-S9).

In samples without LOH (20% of control and 10% of targeted samples), we were able to call heterozygous SNPs in multiple amplified fragments (G_8.04 and G_C16.05, Fig. 3A). Cases with putative LOH at the locus have heterozygous SNPs in the amplicons covering exons 1 and 5 of the *POU5F1* gene (fragments E1-2, G1 and E4 in Fig. 3A) and homozygous SNPs in between (50% of control and 5% of targeted samples). These putative LOH samples would have had to have a cell isolated from the same embryo that had a detectable SNP(s) anywhere in between these flanking exons (e.g. see samples G_8.03 versus G_8.04 in Fig. S4 or W_C16.03 versus W_C16.04 in Fig. S9). This type of LOH could represent CRISPR-Cas9-induced deletions in the order of ~4kb. Interestingly, this was the most prevalent pattern in control samples (Fig. 3B and Fig. S4), which may indicate the possibility of technical issues due to sequencing or overamplification of one parental allele (see below). Bookended samples have two heterozygous SNPs flanking the cut site but in fragments outside the *POU5F1* locus (0% of control and 15% of targeted samples). These LOH events could represent deletions of lengths between ~7kb (G_C12.03, Fig. S7) and ~12kb (W_C11.04, Fig. S6). Finally, in open-ended samples (30% of control and 70% of targeted samples) it was not possible to find heterozygous SNPs in any of the amplified fragments (G_C8.04, Fig. 3A) or there was one or a few heterozygous SNPs on only one side of the region of interest (W_C16.02, Fig. S9). This was the most common pattern in targeted samples (Fig. 3B and Figs. S5-S9) and could represent large deletions of at least ~20kb in length (the size of the region explored).

As mentioned above, the MiSeq data must be interpreted with caution given the presence of “LOH events” in Cas9 controls. The gDNA employed in these experiments was extracted and amplified with a kit based on multiple displacement amplification (MDA, Methods), which is common in single cell applications but is known to have high allelic dropout and preferential amplification rates (19). Also, we lack the parental genotype of the analysed samples and therefore cannot exclude the possibility that they inherited a homozygous genotype in the explored region. Nevertheless, the fact that there is a significant number of CRISPR-Cas9 targeted samples with the largest LOH patterns is of note (Fig. 3B).

No evidence of on-target complexity using digital karyotype and LOH analysis of the single-cell transcriptome data

The use of RNA sequencing data (RNA-seq) to detect chromosomal abnormalities (20) has great potential to complement the informative low-pass WGS or array CGH methods currently used for embryo screening in the context of assisted reproductive technologies (21, 22). In addition to karyotype analysis, transcriptome data may also provide information about embryo competence at the molecular level. In fact, Groff and colleagues have shown that it is possible to estimate whether a chromosome was gained or lost in a sample based on significant variations in its total gene expression compared to other samples (21). In addition, Weissbein *et al.* developed a pipeline, called eSNP-karyotyping, for the detection of LOH in chromosome arms (23). eSNP-karyotyping is based on measuring the ratio of expressed heterozygous to homozygous SNPs. We applied these two approaches, hereinafter referred to as z-score- and eSNP-karyotyping, to the single-cell RNA-seq (scRNA-seq) samples (distinguished with the prefix T_) that were obtained using the G&T-seq protocol (14)

(Table S3). This allowed us to investigate whether the transcriptome data could be used to determine the frequency of LOH events in CRISPR-Cas9 targeted embryos.

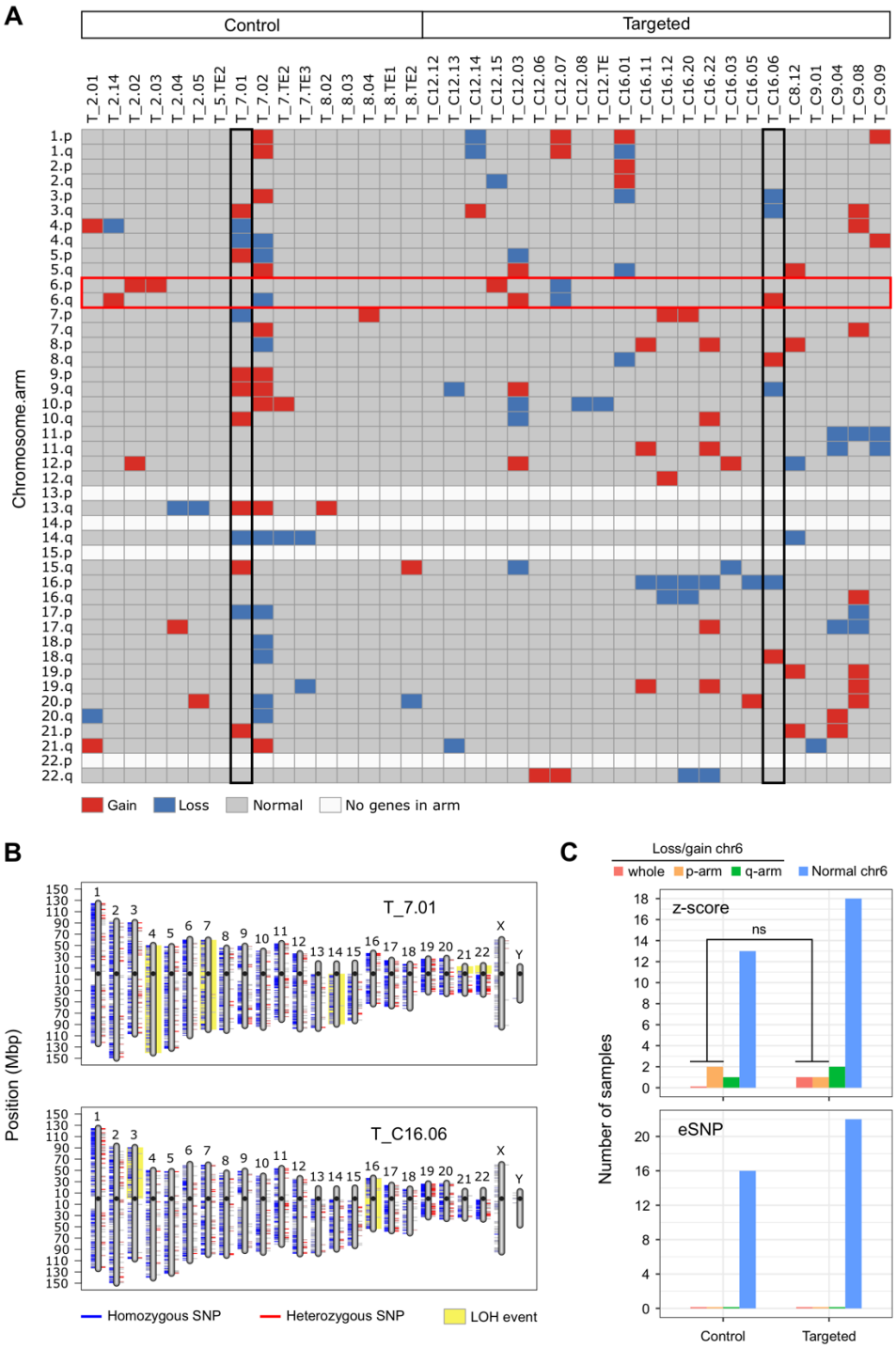

Fig. 4. Transcriptome-based karyotypes do not capture segmental losses/gains of chromosome 6 in OCT4-targeted embryo samples. *(A)* Digital karyotype based on the total gene expression deviation from the average of each chromosome arm (z-score-karyotyping). Chromosome 6 and two samples have been highlighted. *(B)* The loss-of-heterozygosity (LOH) profile of the two samples highlighted in A. These profiles were constructed with the eSNP-karyotyping pipeline, which is also transcriptome-based. Note that the chromosome losses identified by this method were also captured by the karyotype in A. *(C)* The number of control and targeted samples with segmental losses/gains of chromosome 6 according to their transcriptome-based karyotype (see A and B). The reported p-value is the result of a one-tailed Fisher's test.

Since eSNP-karyotyping relies on SNP calls from gene expression data, it is very sensitive to depth and breadth of sequencing (23). Therefore, we used results from this method as a reference to select high quality samples for our transcriptome-based analyses (Fig. S10A-C). After these filtering steps, we retained 38 samples (22 CRISPR-Cas9 targeted and 16 Cas9 controls) to analyse further.

In general, we found good agreement between the chromosomal losses detected by z-score-karyotyping and the LOH events identified by eSNP-karyotyping (Fig. 4A and 4B). For example, the digital karyotype of Fig. 4A shows the loss of chromosome 4, the p-arm of chromosome 7 and the q-arm of chromosome 14 in sample T_7.01, as well as the loss of chromosome 3 and the p-arm of chromosome 16 in sample T_C16.06. These abnormalities are identified as LOH events in the eSNP-karyotyping profiles of the same samples (Fig. 4B). Moreover, the copy number profiles built from low-pass WGS data for different cells from the same embryos also corroborates these chromosomal abnormalities (Fig. S10D and S10E). In terms of events that could be associated with CRISPR-Cas9 on-target damage, z-score-karyotyping identified the loss of chromosome 6 in sample T_C12.07 (Fig. 4A), which is consistent with the open-ended LOH pattern observed in the gDNA extracted from the same cell G_C12.07 (Fig. S7) and the segmental loss detected in sample L_C12.01 from the same embryo (Fig. 2B). Also, the gain of the p-arm of chromosome 6 was detected in sample T_C12.15 (Fig. 4A), which is consistent with the segmental gain observed in sample L_C12.02 from the same embryo (Fig. 2B). The gains and losses of chromosome 6 in samples T_2.02, T_2.03, T_2.14, T_7.02 and T_C16.06 (Fig. 4A) are difficult to interpret due to the low quality of their MiSeq data or the lack of amplicon information for the q-arm (Fig. S4 and Fig. S9). Interestingly, eSNP-karyotyping did not detect any LOH events in chromosome 6 (Fig. S11), suggesting that this approach is not sensitive enough to detect segmental abnormalities in single cell samples. Overall, the transcriptome-based karyotypes did not confirm the trends observed in the gDNA-derived data (Fig. 4C).

Discussion

In all, we reveal unexpected on-target complexity following CRISPR-Cas9 genome editing of human embryos. Our data suggest approximately 22% of samples exhibit segmental losses/gains adjacent to the *POU5F1* locus and LOH events that span 4kb to at least 20kb. Chromosome instability, including whole or segmental chromosome gain or loss, is common in human preimplantation embryos (24, 25). However, in contrast to Cas9 control embryos, we noted a significantly higher frequency of CRISPR-Cas9 targeted embryos with a segmental gain or loss that was directly adjacent to the *POU5F1* on-target site. The segmental errors were observed in embryos from distinct genetic backgrounds and donors. Therefore, together with their on-target location, this suggests that the errors may have been an unintended consequence of CRISPR-Cas9 genome editing. This is supported by the frequencies of LOH we observed using an independent targeted deep-sequencing approach. However, due to the nature of our datasets (shallow sequencing, MDA-amplified gDNA, lack of parental genotypes) we may be overestimating LOH events. It is important to note that 55.6% of CRISPR-Cas9 targeted cells did not exhibit any obvious segmental or whole chromosome 6 abnormalities, indicating that their genotype and phenotype, with respect to OCT4 function, are interpretable. Given the likelihood of mosaicism, it is unclear whether the segmental abnormalities we observed in any one cell

analysed from each embryo are representative of the entire CRISPR-Cas9 targeted embryo or a subset of cells within the embryo. Altogether, this points to the need to develop a robust technique to distinguish cells and embryos affected by CRISPR-Cas9 unintended damage from correctly edited embryos.

By contrast, we did not observe significantly more abnormalities on chromosome 6 using methods to determine LOH or karyotype from scRNA-seq datasets. There are several factors that could account for the discrepancy between these datasets. Firstly, we do not have the transcriptome from the same samples that showed gains and losses of chromosome 6 in the cytogenetics analysis. A follow-up study in which both transcriptomics and cytogenetics data are extracted from the same sample would be very informative and could be performed by modifying the G&T-seq (17) to incorporate a multiple annealing and looping-based amplification cycles (MALBAC) method for WGA (26) in place of MDA, which was used here. Secondly, mosaicism is common in human preimplantation embryos (27) and this could explain why the digital karyotypes based on gene expression did not detect abnormalities at the same rate as the copy number profiles. Another possibility is that the LOH events are not sufficiently large to impact total gene expression of chromosome 6, which is what z-score- and eSNP-karyotyping rely on. This could also account for the cytogenetics results, as LOH up to a few Mb in size could cause mapping issues due to the very low coverage of shallow sequencing that are reflected as gains and losses of whole chromosome segments. Finally, the LOH events detected by gDNA-derived data may only affect genes that are not expressed in the embryo context or whose expression is so low that it cannot be accurately measured by scRNA-seq. So, when z-score- and eSNP-karyotyping compare gene or SNP expression of targeted versus control samples, no significant differences are identified.

The segmental aneuploidies identified by cytogenetics analysis (Fig. 2B and S2) most probably point to the occurrence of complex genomic rearrangements in OCT4-targeted samples, such as chromosomal translocations or end-to-end fusions, as it seems unlikely that the rest of the chromosome would continue to be retained without a telomere (28–30). An important next step to gain insights into the extent of the damage would be to use alternative methods. One possibility to understand the complexity would be to perform cytogenetic analysis using fluorescence in situ hybridization (31) to probe for segments of chromosome 6. Another option is a chromosome walk-along approach to amplify genomic fragments even further away from the 20kb genomic region that we evaluated, in order to bookend heterozygous SNPs on either side of the *POU5F1* on-target site. This may be kilo- or mega-bases away from the on-target site based on previous publications in the mouse or human cell lines (9, 10, 12–14). To fully elucidate the LOH that has occurred at the on-target site in our study, and to resolve the controversy over the IH-HR reported by others (8, 9), will require the development of a pipeline to enrich for the region of interest and then perform deep (long-read) sequencing to evaluate the presence and extent of on-target damage. By bookending SNPs on either side of an LOH event, primers could be designed to incorporate the SNPs and ensure that both parental alleles are amplified. However, this is difficult to perform, and alternative methods include using CRISPR gRNAs to cut just outside of the LOH region followed by long-read sequencing (32).

Our re-evaluation of on-target mutations, together with previous accounts of unexpected CRISPR-Cas9 on-target damage (9, 10, 12–14), strongly underscores the importance of further basic research in a number of

cellular contexts to resolve the damage that occurs following genome editing. Moreover, this stresses the importance of ensuring whether one or both parental chromosome copies are represented when determining the genotype of any sample to understand the complexity of on-target CRISPR mutations, especially in human primary cells. The development of a reproducible pipeline to evaluate on-target complexity, especially in single cells, would also be of benefit.

Methods

Ethics statement. We reprocessed the DNA and reanalysed the data generated in our previous study (16) and we did not use any additional human embryo samples for the present work. Human embryos were donated to the previous project by informed consent under UK Human Fertilization and Embryo Authority (HFEA) License number R0162. Approval was also obtained from the Health Research Authority's Cambridge Central Research Ethics Committee, IRAS project ID 200284 (Cambridge Central reference number 16/EE/0067). Informed consent was obtained from all couples that donated surplus embryos following IVF treatment. Before giving consent, donors were provided with all of the necessary information about the research project, an opportunity to receive counselling, and details of the conditions that apply within the license and the HFEA Code of Practice. Specifically, patients signed a consent form authorising the use of their embryos for research including genetic tests and for the results of these studies to be published in scientific journals. No financial inducements were offered for donation. Patient information sheets and the consent documents provided to patients are publicly available (https://www.crick.ac.uk/research/a-z-researchers/researchers-k-o/kathy-niakan/hfea-licence/).

CRISPR-Cas9 targeting of *POU5F1*. The samples that we analysed correspond to single cells or trophectoderm biopsies from human preimplantation embryos that were CRISPR-Cas9 genome edited in our previous study (16). Briefly, *in vitro* fertilised zygotes that were donated as surplus to infertility treatment were microinjected with either a sgRNA-Cas9 ribonucleoprotein complex or with Cas9 protein alone and cultured for 5-6 days (targeted and control samples, respectively). The sgRNA was designed to target exon 2 of the *POU5F1* gene (16). Genomic DNA from Cas9 control and OCT4-targeted human embryos was isolated from either an individual single cell or a cluster of 2-5 cells from trophectoderm biopsies from embryos that developed to the blastocyst stage, as well as blastomeres from earlier stage embryos (Table S2 and S3) using the REPLI-g Single Cell Kit (QIAGEN, 150343) according to the manufacturer's guidelines. Since these samples were originally isolated for further processing by G&T-seq (17) or whole genome amplification, they are identified by a G, T or W prefix in Tables S2 and S3. DNA samples isolated for cytogenetic analysis were isolated and amplified with the SurePlex kit (Rubicon Genomics) and are identified by an L prefix (Table S1).

Cytogenetic analysis. To determine the chromosome copy number of samples in Table S1, their genomic DNA was subjected to low-pass whole genome sequencing (depth of sequencing < 0.1x). Libraries were prepared using the VeriSeq PGS Kit (Illumina) and sequenced with the MiSeq platform as previously described (16). Sequenced reads were aligned to the human genome hg19 using BWA version 0.7.17 (33) and the digital karyotypes were generated with the R package QDNAseq version 1.24.0 (34). We used bins of size 100kb

and filtered out samples with a strong difference between the measured and expected standard deviations of the generated profile (Fig. S1). The expected standard deviation (Eσ) is defined as √1/N, where N is the average number of reads per bin. The measured standard deviation (σ) is calculated from the data with a 0.1%-trimmed first-order estimate (34).

PCR primer design and testing. The 15 PCR primer pairs were designed with the Primer3 webtool (http://bioinfo.ut.ee/primer3/) across the *POU5F1* locus (chr6:31,157,800-31,178,600). We also designed a control primer pair in exon 4 of the gene *ARGFX,* which is on a different chromosome (chr3:121,583,621-121,586,438, Table S4). We restricted the product size to the 150-500bp range and used the following primer temperature settings: Min=56, Opt=58, Max=60. We selected primer pairs with similar melting temperature, length, the lowest possible GC percentage and with amplicons containing at least one common human variation as reported by dbSNP 1.4.2 (https://www.ncbi.nlm.nih.gov/variation/docs/glossary/#common). We tested all primers using 1uL of genomic DNA from H9 human ES cells in a PCR reaction containing 12.5 uL Phusion High Fidelity PCR Master Mix (New England Biolabs, M0531L), 1.25 uL 5 uM forward primer, 1.25 uL 5 uM reverse primer and 9 uL nuclease-free water. Thermocycling settings were: 95°C 5min, 35 cycles of 95°C 30s, 58°C 30s, 72°C 1min, and a final extension of 72°C 5min. We confirmed that the size of the PCR products corresponded to the expected amplicon size (Table S4) by gel electrophoresis.

PCR amplification. In preparation for PCR amplification, the DNA isolated from samples in Table S2 was diluted 1:100 in nuclease-free water. To expedite the processing of our 2192 samples (16 target fragments for each of the 137 DNA templates), we used the QIAgility robot (QIAGEN, 9001531) for master mix preparation (see above) and distribution to 96-well plates using the layout depicted in Table S5 for a total of 24 plates. Then, the Biomek FX liquid handling robot (Beckman Coulter, 717013) was used to transfer 1uL of DNA at once to the master mix plates using a 96-multichannel pipetting head and to mix the reagents. The PCR reaction was run with the thermocycling settings described above. PCR products were cleaned with the Biomek FX robot using the chemagic SEQ Pure20 Kit (PerkinElmer, CMG-458) as per manufacturer's instructions.

Targeted deep sequencing. Clean PCR amplicons from the same DNA sample were barcoded and pooled to generate 137 barcoded libraries that were submitted for targeted deep sequencing by Illumina MiSeq v3 (300bp paired end reads).

SNP-typing. We trimmed the MiSeq paired-end reads with DADA2 (35) to remove low-quality regions (function filterAndTrim with parameters trimLeft=5, truncLen=c(150,150), truncQ=2, maxN=0 and maxEE=c(5, 5)). Then, we corrected substitution errors in the trimmed reads with RACER (36) and mapped the corrected reads to the human genome hg38 with BWA version 0.7.17 (33) in multi-threaded mode using the mem algorithm with default settings. Subsequently, SAM files were converted to the BAM format and post-processed (sorting, indexing and mate fixing) using Samtools version 1.3.1 (37). SNP calling was performed with BCFtools version 1.8 (38) using the mpileup (--max-depth 2000 -a 'AD,DP,ADF,ADR' -Ou) and call (-mv -V 'indels' -Ov) algorithms in multi-threaded mode. Since the average length of our amplicons is 300bp and the trimmed reads ended up having length ~145, at least 10 reads are needed to achieve a 5x coverage at each amplicon.

Therefore, SNPs supported by less than 10 reads and with mapping quality below 50 were filtered out. The resulting VCF files were then indexed and inspected in the Integrative Genomics Viewer (39).

scRNA-seq data analysis. scRNA-seq reads from G&T-seq samples (Table S3) were aligned to the human reference genome GRCh38 using TopHat2 version 2.1.1 (40). Samples with a breadth of sequencing below 0.05 were not considered for any downstream analysis (Fig. S9A-C). Read counts per gene were calculated using HTSeq 0.12.4 (41) and normalised using TPM units (42). For digital karyotyping based on gene expression, we adapted the method described in (21) to identify gains or losses of chromosomal arms. Briefly, after removal of no-show, mitochondrial, sex chromosome and PAR genes, the TPM expression of all genes mapping to the p-arm of chromosome *i* was summed and compared to the average sum for the same chromosome and arm across samples via the calculation of a z-score. Z-scores with values below -1.65 and above 1.65 were considered segmental losses and gains, respectively. Chromosome arms with values in between were considered to be normal. The same procedure was repeated for the q-arm of each chromosome. For digital karyotyping based on SNP expression, we applied the eSNP-Karyotyping pipeline with default parameters (23). eSNP-Karyotyping identifies loss-of-heterozygosity in a chromosome arm when the ratio of heterozygous to homozygous SNPs in that arm is significantly lower compared to the other chromosome arms. For this, the pipeline employs the GATK best practices for SNP calling using RNA-seq data and compares called heterozygous variants with homozygous variants reported on dbSNP 1.4.2 (23). eSNP-karyotyping is very sensitive to depth and breadth of sequencing, so we selected samples for our scRNA-seq analyses based on the quality of the eSNP-karyotyping profiles (Fig. S10A-C and Table S3).

Data and software availability. All data supporting the findings of this study are available within the article and its supplementary information or from the corresponding author upon reasonable request. MiSeq and low-pass WGS data have been deposited to the Sequence Read Archive (SRA) under accession number PRJNA637030. scRNA-seq data was extracted from the Gene Expression Omnibus (GE) using accession GSE100118. A detailed analysis pipeline is available at the following site: https://github.com/galanisl/loh_scripts.

Acknowledgements

We thank the generous donors whose contributions have enabled this research. We thank Robin Lovell-Badge, Alexander Frankell, Maxime Tarabichi, the Niakan and Turner laboratories for discussion, advice and feedback; the Francis Crick Institute's core facilities including Jerome Nicod and Robert Goldstone at the Advanced Sequencing Facility; D.W. was supported by the National Institute for Health Research (NIHR) Oxford Biomedical Research Centre Programme. N.K. was supported by the University of Oxford Clarendon Fund and Brasenose College Joint Scholarship. Work in the K.K.N. and J.M.A.T. labs was supported by the Francis Crick Institute, which receives its core funding from Cancer Research UK (FC001120 and FC001193), the UK Medical Research Council (FC001120 and FC001193), and the Wellcome Trust (FC001120 and FC001193). Work in the K.K.N. laboratory was also supported by the Rosa Beddington Fund.

Author contributions

K.K.N. conceived the project. N.M.E.F. generated the genomics and transcriptomics datasets. A.M., E.H. and G.A-L. designed and tested primers. N.K. and D.W. generated the low-pass WGS data. M.G. performed the PCR amplification experiments with the robotics equipment. J.Z. implemented the variant calling pipeline for the amplicon sequencing data. G.A-L. collected, processed and analysed all the datasets. J.M.A.T. provided advice on the project design. G.A-L. and K.K.N. wrote the manuscript with the help from all other authors. All authors assisted with experimental design and figures.

References

1. M. Adli, The CRISPR tool kit for genome editing and beyond. *Nature Communications* **9**, 1911 (2018).
2. R. A. Lea, K. K. Niakan, Human germline genome editing. *Nature Cell Biology* **21**, 1479–1489 (2019).
3. National Academy of Sciences and National Academy of Medicine and National Academies of Sciences, Engineering, and Medicine, *Human Genome Editing: Science, Ethics, and Governance* (The National Academies Press, 2017).
4. Nuffield Council on Bioethics, *Genome editing and human reproduction: social and ethical issues* (Nuffield Council on Bioethics, 2018).
5. P. Liang, *et al.*, CRISPR/Cas9-mediated gene editing in human tripronuclear zygotes. *Protein & Cell* **6**, 363–372 (2015).
6. X. Kang, *et al.*, Introducing precise genetic modifications into human 3PN embryos by CRISPR/Cas-mediated genome editing. *Journal of Assisted Reproduction and Genetics* **33**, 581–588 (2016).
7. L. Tang, *et al.*, CRISPR/Cas9-mediated gene editing in human zygotes using Cas9 protein. *Molecular Genetics and Genomics* **292**, 525–533 (2017).
8. H. Ma, *et al.*, Correction of a pathogenic gene mutation in human embryos. *Nature* **548**, 413–419 (2017).
9. D. Egli, *et al.*, Inter-homologue repair in fertilized human eggs? *Nature* **560**, E5–E7 (2018).
10. F. Adikusama, *et al.*, Large deletions induced by Cas9 cleavage. *Nature* **560**, E8–E9 (2018).
11. H. Ma, *et al.*, Ma et al. reply. *Nature* **560**, E10–E16 (2018).
12. M. Kosicki, K. Tomberg, A. Bradley, Repair of double-strand breaks induced by CRISPR–Cas9 leads to large deletions and complex rearrangements. *Nature Biotechnology* **36**, 765–771 (2018).
13. G. Cullot, *et al.*, CRISPR-Cas9 genome editing induces megabase-scale chromosomal truncations. *Nature Communications* **10** (2019).
14. D. D. G. Owens, *et al.*, Microhomologies are prevalent at Cas9-induced larger deletions. *Nucleic Acids Research* **47**, 7402–7417 (2019).
15. H. Lee, J.-S. Kim, Unexpected CRISPR on-target effects. *Nature Biotechnology* **36**, 703–704 (2018).
16. N. M. E. Fogarty, *et al.*, Genome editing reveals a role for OCT4 in human embryogenesis. *Nature* **550**, 67–73 (2017).
17. I. C. Macaulay, *et al.*, G&T-seq: parallel sequencing of single-cell genomes and transcriptomes. *Nature Methods* **12**, 519–522 (2015).
18. T. Kishikawa, *et al.*, Empirical evaluation of variant calling accuracy using ultra-deep whole-genome sequencing data. *Scientific Reports* **9**, 1784 (2019).
19. E. Borgström, M. Paterlini, J. E. Mold, J. Frisen, J. Lundeberg, Comparison of whole genome amplification techniques for human single cell exome sequencing. *PLOS ONE* **12**, e0171566 (2017).
20. J. A. Griffiths, A. Scialdone, J. C. Marioni, Mosaic autosomal aneuploidies are detectable from single-cell RNAseq data. *BMC Genomics* **18**, 904 (2017).
21. A. F. Groff, *et al.*, RNA-seq as a tool for evaluating human embryo competence. *Genome Res.* **29**, 1705–1718 (2019).
22. M. Poli, *et al.*, Past, Present, and Future Strategies for Enhanced Assessment of Embryo's Genome and Reproductive Competence in Women of Advanced Reproductive Age. *Frontiers in Endocrinology* **10**, 154 (2019).
23. U. Weissbein, M. Schachter, D. Egli, N. Benvenisty, Analysis of chromosomal aberrations and recombination by allelic bias in RNA-Seq. *Nature Communications* **7**, 12144 (2016).
24. E. Vanneste, *et al.*, Chromosome instability is common in human cleavage-stage embryos. *Nature Medicine* **15**, 577–583 (2009).

25. D. Babariya, E. Fragouli, S. Alfarawati, K. Spath, D. Wells, The incidence and origin of segmental aneuploidy in human oocytes and preimplantation embryos. *Human Reproduction* **32**, 2549–2560 (2017).
26. C. Zong, S. Lu, A. R. Chapman, X. S. Xie, Genome-Wide Detection of Single-Nucleotide and Copy-Number Variations of a Single Human Cell. *Science* **338**, 1622–1626 (2012).
27. R. C. McCoy, Mosaicism in preimplantation human embryos: when chromosomal abnormalities are the norm. *Trends in Genetics* **33**, 448–463 (2017).
28. B. van Steensel, A. Smogorzewska, T. de Lange, TRF2 Protects Human Telomeres from End-to-End Fusions. *Cell* **92**, 401–413 (1998).
29. A. W. I. Lo, *et al.*, Chromosome Instability as a Result of Double-Strand Breaks near Telomeres in Mouse Embryonic Stem Cells. *Molecular and Cellular Biology* **22**, 4836–4850 (2002).
30. R. Capper, *et al.*, The nature of telomere fusion and a definition of the critical telomere length in human cells. *Genes & Development* **21**, 2495–2508 (2007).
31. E. Fragouli, *et al.*, Cytogenetic analysis of human blastocysts with the use of FISH, CGH and aCGH: scientific data and technical evaluation. *Human Reproduction* **26**, 480–490 (2011).
32. T. Gilpatrick, *et al.*, Targeted nanopore sequencing with Cas9-guided adapter ligation. *Nature Biotechnology* **38**, 433–438 (2020).
33. H. Li, R. Durbin, Fast and accurate long-read alignment with Burrows–Wheeler transform. *Bioinformatics* **26**, 589–595 (2010).
34. I. Scheinin, *et al.*, DNA copy number analysis of fresh and formalin-fixed specimens by shallow whole-genome sequencing with identification and exclusion of problematic regions in the genome assembly. *Genome Research* **24**, 2022–2032 (2014).
35. B. J. Callahan, *et al.*, DADA2: High-resolution sample inference from Illumina amplicon data. *Nature Methods* **13**, 581–583 (2016).
36. L. Ilie, M. Molnar, RACER: Rapid and accurate correction of errors in reads. *Bioinformatics* **29**, 2490–2493 (2013).
37. H. Li, *et al.*, The Sequence Alignment/Map format and SAMtools. *Bioinformatics* **25**, 2078–2079 (2009).
38. H. Li, A statistical framework for SNP calling, mutation discovery, association mapping and population genetical parameter estimation from sequencing data. *Bioinformatics* **27**, 2987–2993 (2011).
39. J. T. Robinson, *et al.*, Integrative genomics viewer. *Nature Biotechnology* **29**, 24–26 (2011).
40. D. Kim, *et al.*, TopHat2: accurate alignment of transcriptomes in the presence of insertions, deletions and gene fusions. *Genome Biology* **14**, R36 (2013).
41. S. Anders, P. T. Pyl, W. Huber, HTSeq--a Python framework to work with high-throughput sequencing data. *Bioinformatics* **31**, 166–169 (2015).
42. G. P. Wagner, K. Kin, V. J. Lynch, Measurement of mRNA abundance using RNA-seq data: RPKM measure is inconsistent among samples. *Theory in Biosciences* **131**, 281–285 (2012).